

Optical study of the stoichiometry-dependent electronic structure of TiC_x , VC_x , and NbC_x

T. Koide and T. Shidara

Photon Factory, National Laboratory for High Energy Physics, Tsukuba, Ibaraki 305, Japan

H. Fukutani

Institute of Physics, Tsukuba University, Tsukuba, Ibaraki 305, Japan

A. Fujimori

Department of Physics, Faculty of Science, University of Tokyo, Tokyo 113, Japan

T. Miyahara and H. Kato

Photon Factory, National Laboratory for High Energy Physics, Tsukuba, Ibaraki 305, Japan

S. Otani and Y. Ishizawa

National Institute for Research in Inorganic Materials, Tsukuba, Ibaraki 305, Japan

(Received 6 February 1990)

The stoichiometry-dependent bulk electronic structure has been studied by optical spectroscopy for single crystals of TiC_x with $x = 0.95$ and 0.70 , VC_x with $x = 0.86$ and 0.76 , and NbC_x with $x = 0.93$, 0.84 , and 0.71 . The reflectance was measured in the energy range $0.5\text{--}40$ eV for all of the samples and up to 100 eV for $\text{TiC}_{0.95}$, $\text{VC}_{0.86}$, and $\text{NbC}_{0.93}$. By correcting for the surface-roughness effect using the measured roughness values, the data were Kramers-Kronig analyzed to obtain the dielectric function and related functions. The observed interband transitions have been interpreted on the basis of existing calculations for the energy-band structure and partial density of states. The main peaks above 4 eV were assigned to transitions at and around the X and Q portions in the Brillouin zone. Their shifts to lower energy and reduced intensities with decreasing carbon concentration are discussed in terms of p - d hybridization. Features arising from transitions involving the initial or final states near the Fermi level were observed in the low-energy region. Their dramatic stoichiometry-dependent behavior provides clear experimental evidence that the Fermi level moves downward in VC_x and NbC_x with lowering carbon content. A structure that develops remarkably in intensity as x decreases appears around 2 eV in VC_x and NbC_x , while no counterpart is discernible in TiC_x . This feature can be attributed to a transition between vacancy-induced states with a_{1g} and t_{1u} symmetries. The contribution of the metal p state to the optical spectra is discussed in relation to both the intrinsic peaks and the vacancy-induced feature. The electron-energy-loss functions show distinct plasmon structures that weaken and shift to lower energy with decreasing x . The main volume plasmon peak is close to the free-electron-gas plasmon energy. A small Drude plasma structure has been observed at 2.7 eV in $\text{NbC}_{0.93}$, being rapidly attenuated with increasing carbon vacancies.

I. INTRODUCTION

The group-IVB and -VB transition-metal carbides and nitrides exhibit interesting and unique bonding properties.^{1,2} Their extreme hardness and high melting temperatures are typical of covalently bonded materials, leading to uses as coatings for cutting tools, wear-resistant surfaces, and refractory materials. These compounds also show metallic properties such as color, good conductivity, and, in some cases, superconductivity. In addition, they mostly crystallize in the rock-salt ($B1$) structure typical of ionic crystals, with nonmetal atoms located in the octahedral interstitial positions of the metal face-centered-cubic (fcc) sublattice. Another remarkable property of this class of materials is their tendency to form nonstoichiometrically;^{1,2} they can accommodate up to 50% vacancies on a nonmetal sublattice while retain-

ing the rock-salt phase in thermodynamic equilibrium. Though the vacancies are normally randomly distributed, they occasionally exhibit a short- or long-range order, thus forming vacancy clusters or superlattices. The introduction of vacancies has a strong influence on a variety of physical properties, e.g., superconductivity-transition temperature, specific heat, paramagnetic susceptibility, and melting temperature.^{1,2}

The extraordinary properties are closely related to the electronic structure and have stimulated a large number of studies. Theoretically, following the pioneering work of Bilz,³ who calculated a tight-binding (TB) band for TiC , many band-structure calculations have been performed for stoichiometric compounds. Summaries of band calculations have been given in review articles by Calais,⁴ Neckel,⁵ and Schwarz.⁶ The augmented-plane-wave⁷⁻¹⁰ (APW) and the linearized APW (LAPW) (Refs.

11–14) methods were extensively used, in particular by Neckel, Schwarz, and collaborators. Most of the band calculations indicate the following: (i) The energetically lower part of the valence-conduction bands is formed mainly from nonmetal $2p$ states strongly hybridized with metal d states (nonmetal p bands), which is the origin of the strong covalent bonding; (ii) the higher part of the valence-conduction bands is built up from metal d states with some admixture of the nonmetal $2p$ character (metal d bands); (iii) the Fermi level (E_F) for the IVB transition-metal carbides is located at the deep minimum in the density of states (DOS) between the p and d bands, shifting upward into the d bands for other compounds; (iv) the metal s band lies above the d bands while the nonmetal $2s$ band is well below E_F , separated by an energy gap from the p bands; (v) there is a charge transfer from the metal to the nonmetal, reflecting the ionic component of bonding. This picture has been confirmed to be qualitatively correct for stoichiometric compounds by spectroscopic studies such as x-ray and ultraviolet photoelectron spectroscopy (XPS and UPS),^{15–25} optical reflection spectroscopy,^{26–35} x-ray-emission spectroscopy (XES),^{36–41} electron-energy-loss spectroscopy (ELS),^{23,42–44} and bremsstrahlung-isochromat spectroscopy (BIS).⁴⁵ Recent angle-resolved photoemission (ARPES),^{46–59} spin-resolved ARPES,⁶⁰ and angle-resolved inverse photoemission⁶¹ (ARIPES) studies on single-crystal samples have given more detailed information about the location of some critical points and band dispersion along some of the symmetry lines in the Brillouin zone. However, most of these band mappings were made only along the Γ - X line, i.e., [100], because the presence of one- or three-dimensional density-of-states features prohibited an unambiguous determination of critical points in terms of direct transitions, except for the (100) face. Furthermore, appreciable quantitative discrepancies were found between theory and experiment; in general, the experimentally determined bands are deeper below the Fermi level and smaller in dispersion than the calculated bands.^{46–59} Thus, more detailed experimental studies are motivated in order to arrive at a better understanding of the bonding nature of these compounds.

The effects of nonmetal vacancies on the electronic structure have recently gained increasing interest, but understanding lags far behind that for stoichiometric compounds. One fundamental and difficult problem in the theoretical treatment of vacancies is a proper description of vacancy ordering. This vacancy problem has not been exactly solved so far, and essentially three different approximations have been made. The first approach involves cluster models without a nonmetal atom at the center.^{38,62–65} The second involves a direct application of band-calculation algorithms to an entirely ordered array of vacancies.^{66–69} The third uses alloy calculations^{70–78} for randomly distributed vacancies, mainly with a coherent-potential approximation (CPA).^{70–75} A general qualitative agreement has been obtained only for the decrease in the DOS of the nonmetal s and p bands with increasing substoichiometry. Many of the recent calculations predict vacancy-induced DOS peaks near E_F for nonstoichiometric compounds,^{62,63,66–69,72–78}

whereas the TB-CPA results show no such peaks.^{70,71} Agreement is poor regarding the number, energy position, and orbital character of the vacancy states. The results for the carbon-concentration dependence of E_F and the DOS at E_F , which play crucial roles in determining many physical properties, are more confusing, because these values are sensitive to the parameters used in the calculations.

Recent careful XPS,^{17–20,40} UPS,^{20,24,25} and XES (Refs. 38–40) studies have found an occupied vacancy state below E_F , though its observation by angle-resolved ultraviolet photoemission spectroscopy (ARUPS) was made only very recently.^{50,51,54–57,59,60} Investigations by optical spectroscopy³⁵ and ELS (Refs. 42 and 44) have also suggested the existence of vacancy states. Concerning the orbital character of the filled vacancy state, Bringans and Höchst²⁵ observed no resonant enhancement for the vacancy peak in the UPS spectra for $\text{TiN}_{0.80}$ and $\text{ZrN}_{0.82}$ above the Ti $3p$ and Zr $4p$ thresholds, and claimed that the state has little d character, whereas Lindström *et al.*^{50,51,57} have reported some resonant behavior in several nitrides. From XES, XPS, and UPS studies, Beauprez *et al.*^{20,39,40} have recently shown that the metal p state makes an important contribution to the observed vacancy peak, in agreement with the calculated spectra. Little experimental evidence has been obtained as yet for shifts in E_F (Ref. 39) with increasing substoichiometry; this could be partly due to the poor energy resolution in the previous experiments. These studies were mainly concerned with the states near E_F , and only a few systematic studies have been performed on the vacancy-concentration dependence of the overall electronic structure. This is primarily due to a scarcity of well-characterized bulk substoichiometric samples. For example, ARUPS is not very informative for investigations of the vacancy-content-dependent bulk electronic structure, since it is highly surface sensitive; a well-defined surface composition is difficult to prepare for substoichiometric samples.^{24,25,46,79} In contrast, optical spectroscopy is most suited for studying the bulk electron structure of substoichiometric compounds, since it is bulk sensitive and gives information about the electronic states relevant to optical transitions. In addition, it has the advantage of allowing high-resolution measurements. Though several optical-reflectance studies have been reported so far,^{26–35} most were made over a narrow energy region or within a limited range of substoichiometry. Moreover, the previous results for TiC_x do not agree with each other.^{26,27,29,31,32}

In this paper we report on a systematic optical study of well-characterized single-crystal samples of TiC_x , VC_x , and NbC_x over a wide energy range from 0.5 to 40 eV. Measurements are extended up to 100 eV for near-stoichiometric samples, allowing a reliable Kramers-Kronig analysis. Comparisons are made between the present results and reported calculations as well as previous experiments with special interest concerning the influence of the nonmetal vacancies on the electronic structure. Regarding VC_x , reflectance spectra are presented for the first time.

II. EXPERIMENTAL DETAILS

A. Sample preparation and characterization

Crystal rods of TiC_x , VC_x , and NbC_x consisting of single phases and with composition homogeneity within 1% were prepared by a floating-zone technique, the details of which were previously reported.⁸⁰ The carbon-to-metal ratio was determined by chemical analysis with an accuracy better than 1%. We note that it is impossible to prepare VC_x for x larger than 0.88.^{1,2} The ordering of carbon vacancies or the crystal phase was checked by x-ray diffuse scattering and x-ray powder diffraction methods. A short-range ordering was observed in $\text{NbC}_{0.71}$ and a V_8C_7 long-range-ordered phase was seen in $\text{VC}_{0.86}$. The results of the sample characterization are summarized in Table I.

Disks 8–10 mm in diameter and ~ 1 mm in thickness were cut from the crystal rods. They were mechanically polished to optical surfaces using diamond paste as fine as $0.5 \mu\text{m}$ with water as the carrier. The surface roughness of the samples was measured with a digital optical profiler (Zygo Corp., Heterodyne Profiler-5500) using a laser interferometric technique. The measurements were made two times on the central part of the surface. The measured root-mean-square (rms) roughness values are also given in Table I. The samples were washed in acetone, rinsed in ethanol, and dried in a stream of hot air just before measurements.

B. Reflectance measurements

The near-normal-incidence reflectance was measured at room temperature over a photon-energy range between

0.5 and 40 eV for all samples. Measurements were also carried out up to 100 eV for near-stoichiometric samples: $\text{TiC}_{0.95}$, $\text{VC}_{0.86}$, and $\text{NbC}_{0.93}$.

From 0.5 to 6 eV, tungsten and deuterium-discharge lamps were used as light sources, combined with an 0.5-m monochromator with a 600- or 300-lines/mm grating. Two photomultipliers were used as detectors over the 1–6-eV range and a PbS cell in the 0.5–1.5-eV region. Several suitable filters were used to eliminate higher-order light. Light reflected from a quartz-plate beam splitter placed behind the exit slit of the monochromator was monitored so as to compensate for any variation with time of the incident light intensity. In order to avoid any error arising from the position dependence of the detector sensitivity, a sliding-type sample holder was used which allowed intensity measurements of light reflected from both the sample and a quartz plate without any change in the beam position at the detector. The reflectance of the sample was obtained from the known values of the optical constants of quartz. This allowed us to achieve a measurement accuracy as good as 1% of R between 1 and 5.5 eV. When using the PbS cell, a lock-in technique was used in combination with a light chopper in order to suppress the dark current of the detector.

From 4 to 100 eV the measurements were made using synchrotron radiation from the 2.5-GeV storage ring at the Photon Factory, National Laboratory for High Energy Physics. A 1-m Seya-Namioka monochromator on beamline BL-11C was used for the 4–40-eV range. The reflectometer was maintained at a pressure of $\sim 5 \times 10^{-9}$ Torr during the measurements. A photomultiplier coated with sodium salicylate was used as a detector. A 1-mm-thick quartz plate (4–7 eV), an 0.7-mm-thick LiF plate (6–12 eV), and a 200-nm-thick In foil (11.5–16.5 eV) were used as filters to eliminate higher-order light. All

TABLE I. Characteristics of the samples used in this work.

Sample	Nonmetal to metal ratio	Vacancy ordering or phase	Surface roughness σ_{rms} (Å)	
$\text{TiC}_{0.95}$	0.950 ± 0.008		1.5	1.7 (av)
			1.9	
$\text{TiC}_{0.70}$	0.700 ± 0.008		1.8	2.0 (av)
			2.1	
$\text{VC}_{0.86}$	0.858 ± 0.008	V_8C_7 phase	7.5	7.4 (av)
			7.2	
$\text{VC}_{0.76}$	0.758 ± 0.008		11.1	11.0 (av)
			10.8	
$\text{NbC}_{0.93}$	0.930 ± 0.008		10.2	9.2 (av)
			8.1	
$\text{NbC}_{0.84}$	0.844 ± 0.008	probably short-range ordering	6.6	8.5 (av)
			10.3	
$\text{NbC}_{0.71}$	0.712 ± 0.008	short-range ordering	6.1	5.4 (av)
			4.7	

spectra were normalized by the photocurrent from a Au mesh placed behind the entrance slit of the monochromator, which compensated for possible time-dependent changes in the incident flux from the storage ring. The accuracy of the measurements in this region is estimated to be within 3–4 % of R . For the range 25–100 eV, a 2-m constant-deviation monochromator⁸¹ on beamline BL-11D was used. Another reflectometer used did not allow *in situ* measurements of the incident and reflected light intensities; thus, only the relative reflectance was measured. No filters were used for this region. The experimental chamber had a pressure of $\sim 5 \times 10^{-10}$ Torr during the measurements.

III. RESULTS

The reflectance spectra of TiC_x , VC_x , and NbC_x are shown in Figs. 1–3, respectively. The insets display the spectra in the higher-energy region for near-stoichiometric samples: $\text{TiC}_{0.95}$, $\text{VC}_{0.86}$, and $\text{NbC}_{0.93}$. The data for the near-stoichiometric samples from 25 to 100 eV have been scaled to best match at 30 eV the data taken between 4 and 40 eV. Spectral features are labeled for convenience in later discussions.

Surface irregularities cause diffuse scattering, resulting in a reduction of the specular reflectance. The measured normal-incidence reflectance R_s is related to the reflectance R of a perfectly smooth surface by⁸²

$$R_s = R \exp[-(4\pi\sigma_{\text{rms}}/\lambda)^2], \quad (1)$$

where σ_{rms} is the rms surface roughness and λ is the wavelength of light. This formula is valid in the scalar

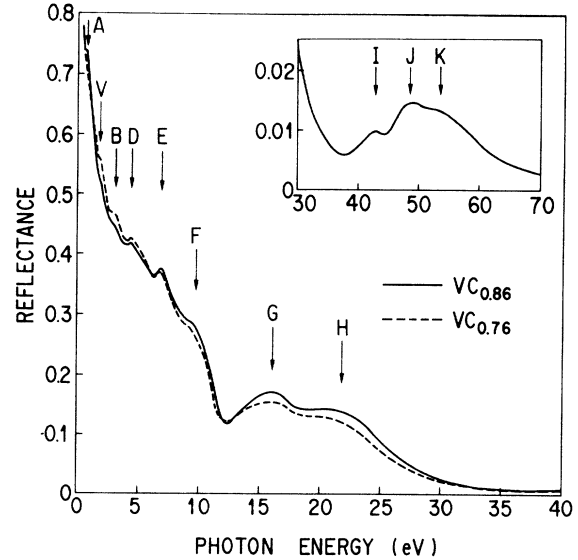


FIG. 2. Reflectance spectra of VC_x with $x=0.86$ and 0.76 . The inset shows the reflectance of $\text{VC}_{0.86}$ in the high-energy region.

approximation for which the phase errors introduced by the surface roughness are small, i.e., $\sigma_{\text{rms}}/\lambda \ll 1$. Since $\sigma_{\text{rms}} \lesssim 11 \text{ \AA}$ for all the present samples (Table I), this necessary condition is sufficiently well satisfied, even at the short-wavelength limit of the present measurements ($\lambda = 124 \text{ \AA}$). All of the data have been corrected for the surface-roughness effect by using Eq. (1) and the measured roughness values given in Table I.

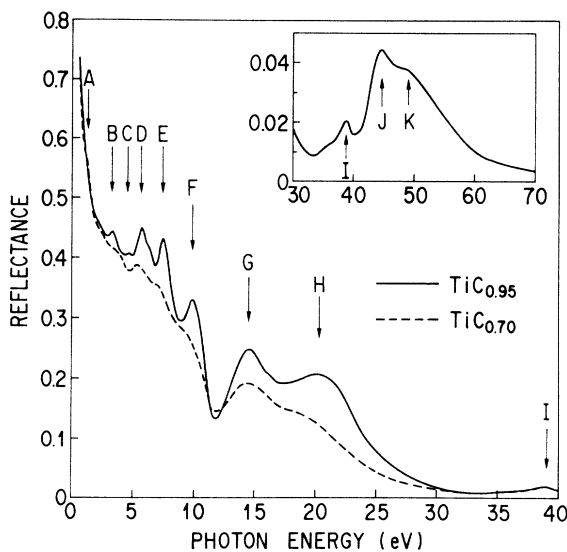


FIG. 1. Reflectance spectra of TiC_x with $x=0.95$ and 0.70 . The inset shows the reflectance of $\text{TiC}_{0.95}$ in the high-energy region.

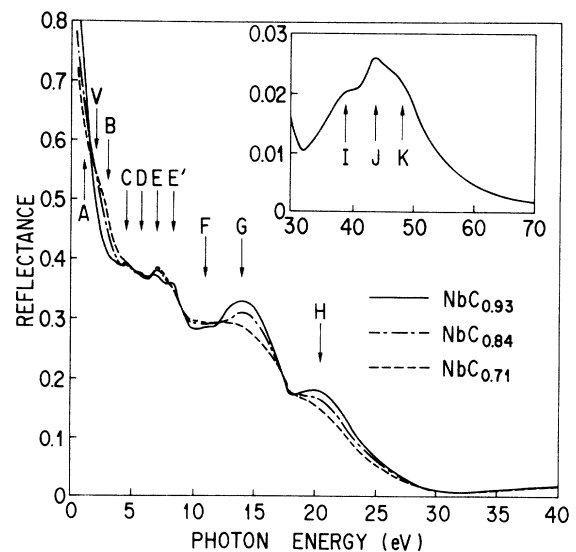


FIG. 3. Reflectance spectra of NbC_x with $x=0.93$, 0.84 , and 0.71 . The inset shows the reflectance of $\text{NbC}_{0.93}$ in the high-energy region.

Three compounds exhibit similar overall spectral characteristics. The reflectance in the region below 2 eV drops off sharply from high values at 0.5 eV with increasing photon energy. Several distinct structures are visible between 2 and 10 eV, followed by broad maxima in the 10–25-eV region, beyond which R decreases steadily to a minimum around 30 eV. Above 35 eV, the reflectance of $\text{TiC}_{0.95}$, $\text{VC}_{0.86}$, and $\text{NbC}_{0.93}$ rises to exhibit multiplet structures (I , J , and K) arising from $\text{Ti } 3p$, $\text{V } 3p$, and $\text{Nb } 4p$ core excitations.

From 4 to 30 eV, most of the structures, C – H , persist to exist over the range of stoichiometry studied, showing a general tendency to become less prominent and to shift to lower energy as the carbon concentration decreases. Stoichiometry-dependent changes are most remarkable for TiC_x and are far less so for NbC_x . The spectral features are very similar for $\text{TiC}_{0.70}$ and VC_x , whereas some differences are noted for NbC_x ; structures in NbC_x are generally broader than those in TiC_x and VC_x and, in addition, a deep minimum at 11–12 eV observed for TiC_x and VC_x is absent for NbC_x .

In the region below 4 eV, a marked stoichiometry dependence is observed for NbC_x , while only a slight carbon-concentration dependence is seen for TiC_x . This

is in sharp contrast to the behavior above 4 eV. In order to see this more clearly, we present the low-energy spectra in expanded scales in Figs. 4–6. For TiC_x , previous data^{26,27,29,31,32,44} are also shown for a comparison in Fig. 4(b). Peak A is present in TiC_x over the range $0.70 \leq x \leq 0.95$. Its counterpart is also visible in $\text{VC}_{0.86}$, but disappears upon going to $\text{VC}_{0.76}$. In NbC_x , in contrast, feature A shows up for $x=0.84$ and 0.71 , whereas there is no sign of the corresponding structure for $x=0.93$. This structure in $\text{VC}_{0.86}$ is located close to the low-energy limit of the present measurement and only a careful search revealed its existence. Feature V depends largely upon stoichiometry and the metal element. The structure is observed in VC_x and grows substantially with decreasing carbon content, while no counterpart is seen in TiC_x . In NbC_x , feature V develops remarkably as x decreases from 0.84 to 0.71, although the structure is not discernible for $x=0.93$. Feature B is distinctly visible in TiC_x , broadening, weakening, and shifting to higher energy with lowering x . The counterpart is only faintly observed in $\text{VC}_{0.86}$, but is clearly seen in $\text{VC}_{0.76}$. Structure B is not discernible in $\text{NbC}_{0.93}$ and $\text{NbC}_{0.84}$, while there is an indication of the structure in $\text{NbC}_{0.71}$ overlapping feature V . These low-energy characteristics indicate stoichiometry-dependent changes in the electronic structure near E_F and in E_F itself.

The reflectance spectra of TiC_x have been studied by a variety of workers,^{26,27,29,31,32,44} as shown in Fig. 4(b). All of the reported data, including ours, agree only on the existence of peak B . The earlier spectra of Lye and Logothetis²⁶ and Alward *et al.*²⁷ show poor agreement with others, both in spectral features and absolute magnitude, though the former is in good agreement with ours at higher energies [not shown in Fig. 4(b)]. The spectra of

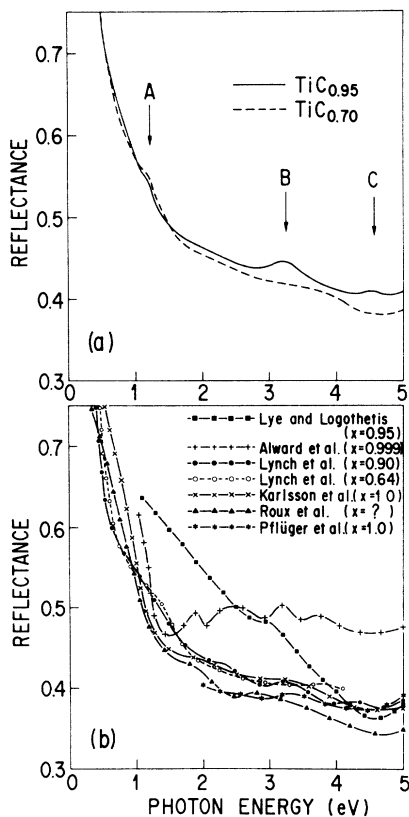


FIG. 4. (a) Reflectance spectra of TiC_x in the low-energy region. (b) Reflectance spectra of TiC_x in the low-energy region reported in the literature (Refs. 26, 27, 29, 31, 32, and 44). The spectrum of Pflüger *et al.* (Ref. 44) was obtained from ELS measurements.

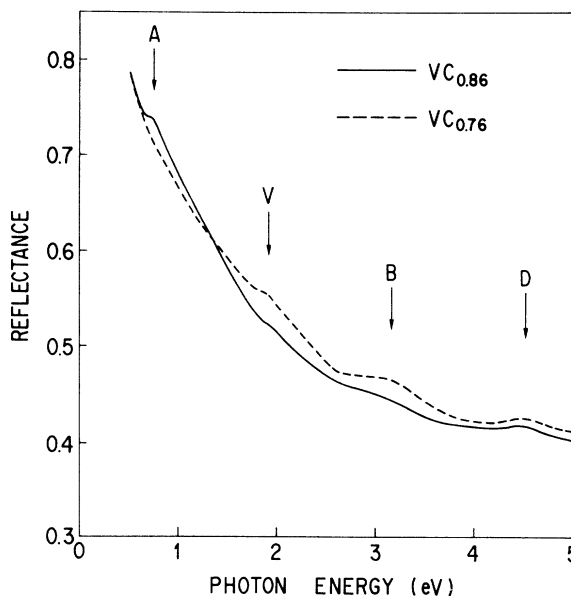


FIG. 5. Reflectance spectra of VC_x in the low-energy region.

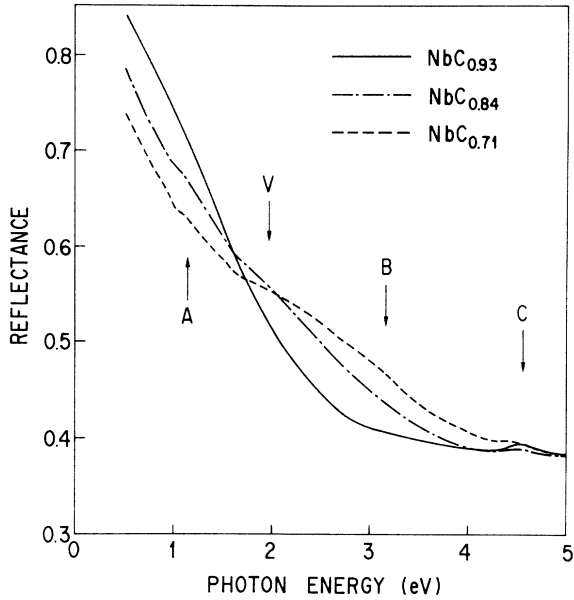


FIG. 6. Reflectance spectra of NbC_x in the low-energy region.

Karlsson *et al.*³¹ and Roux *et al.*³² are less structured than ours, though our data agree reasonably well with theirs regarding absolute magnitude. Lynch *et al.*²⁹ have reported the reflectance spectra of TiC_x in the 0.1–30-eV region. A comparison of our data for $x=0.95$ and 0.70 with theirs for $x=0.90$ and 0.64 shows good agreement over the common energy range, including the stoichiometry dependence. However, even our careful search did not detect any sign of a peak at 2.3 eV, which was visible in their spectrum for $\text{TiC}_{0.90}$.²⁹ No such feature has been observed in other published data as well. Pflüger *et al.*⁴⁴ have presented the reflectance spectrum of $\text{TiC}_{1.0}$ from 2 to 30 eV deduced from the ELS spectrum. Their spectrum is in fairly good agreement with ours for $x=0.95$ and that of Lynch *et al.*²⁹ for $x=0.90$, but does not show peak C. Concerning NbC_x , Allison *et al.*³⁵ have reported the reflectance spectra of NbC_x in the 0.025–11-eV region. Our spectra (Figs. 3 and 6) agree reasonably well with theirs regarding the trends seen as x decreases in the common energy region. However, features A and B are observed, and peaks C, D, E, and E' are better resolved in the present spectra. Pflüger *et al.*⁴⁴ have also reported on the ELS spectra of $\text{NbC}_{1.0}$ and VC_x . Since they did not present the calculated reflectance spectra, no direct comparison is available with our reflectance data.

Kramers-Kronig analyses were made to determine the complex dielectric function $\tilde{\epsilon} = \epsilon_1 + i\epsilon_2$ and related functions from the measured spectra with extrapolation to higher and lower energies. The reflectance below 0.5 eV was assumed to be that of a free-electron gas and was calculated from a parameter fitting to the measured spectra with parameters of the Drude plasmon energy, the relaxation time of the free-electron gas, and the interband correction to the dielectric function. The data for the near-stoichiometric samples in the 25–100-eV region

were used as the reflectance for the nonstoichiometric samples by assuming that the spectral shape is independent of the carbon concentration and by adjusting them in magnitude at 30 eV to the measured data of nonstoichiometric samples from 4 to 40 eV. This assumption should be reasonable since the 40–100-eV region has no carbon core excitations, dominated by transitions from the metal core p to the metal d states. Above 100 eV, the spectra were extrapolated proportionally to E^{-p} with p taken as an adjustable parameter. We previously reported on the optical constants of chemical-vapor-deposited $\text{TiC}_{0.95}$ at given energies over the 80–800-eV range.⁸³ Parameter p was determined to be 4.3 for $\text{TiC}_{0.95}$, so that the result of the Kramers-Kronig transformation may reproduce the same optical constants at 80 eV. The availability of these high-energy data allowed a reliable Kramers-Kronig analysis for $\text{TiC}_{0.95}$; detailed optical constants will be reported elsewhere. A p of 4.3 was also used for $\text{TiC}_{0.70}$. For VC_x and NbC_x no data are available above 100 eV and $p=4$ was chosen from the asymp-

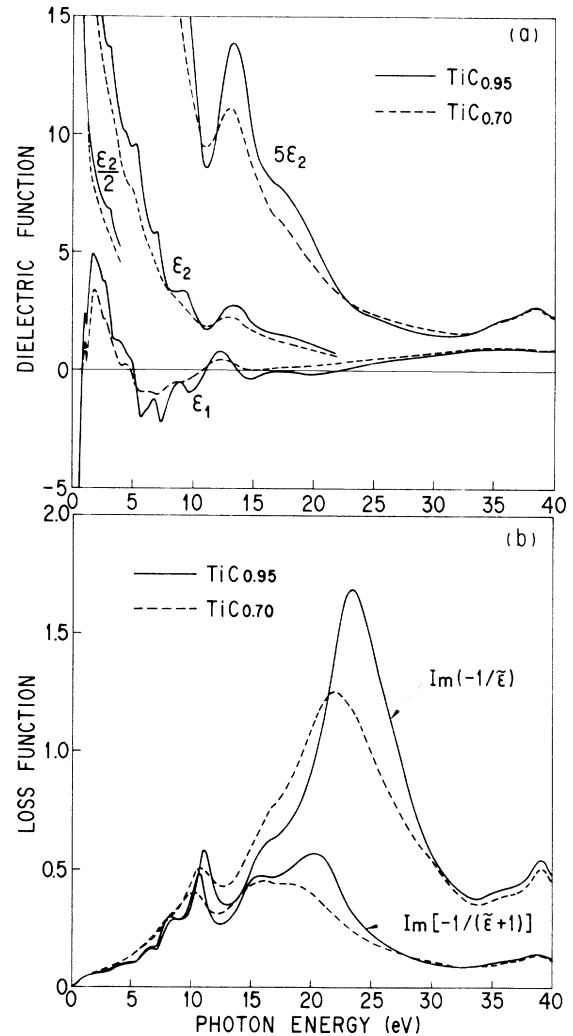


FIG. 7. (a) Real (ϵ_1) and imaginary (ϵ_2) parts of the dielectric function of TiC_x . (b) Electron-energy-loss functions $\text{Im}(-1/\tilde{\epsilon})$ (volume) and $\text{Im}[-1/(\tilde{\epsilon}+1)]$ (surface) of TiC_x .

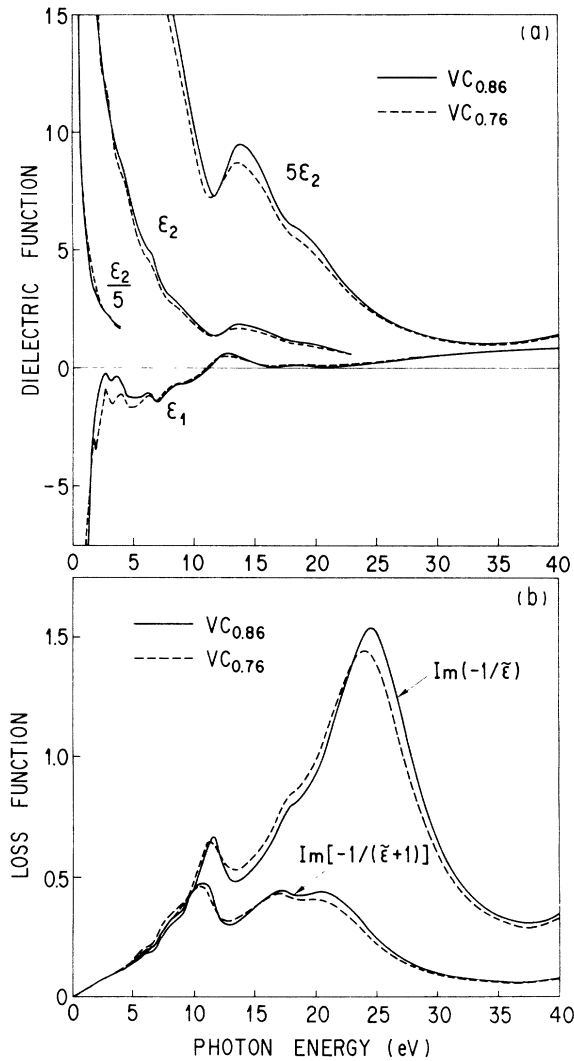


FIG. 8. (a) Real (ϵ_1) and imaginary (ϵ_2) parts of the dielectric function of VC_x . (b) Electron-energy-loss functions $Im(-1/\epsilon)$ (volume) and $Im[-1/(\epsilon+1)]$ (surface) of VC_x .

otic behavior of the measured spectra for the near-stoichiometric samples in the 80–100-eV region.

The results of the Kramers-Kronig analysis are shown in Figs. 7–12. Figures 7–9(a) display the real and imaginary parts of the dielectric function, with the scale for ϵ_2 being expanded for clarity. Figures 7–9(b) show the volume- and surface-electron-energy-loss functions $Im(-1/\epsilon)$ and $Im[-1/(\epsilon+1)]$, respectively. The inset in Fig. 9(b) displays the low-energy volume-loss functions of NbC_x in expanded scales. Figures 10–12 show the optical conductivity, $\sigma = \epsilon_2 E / 4\pi\hbar$. The insets display the high-energy conductivity of $TiC_{0.95}$, $VC_{0.86}$, and $NbC_{0.93}$. A comparison of the dielectric function and the optical conductivity with the reflectance shows that there is a one-to-one correspondence of the interband structures; thus, the conductivity peaks are labeled, corresponding to the features observed in the reflectance spectra. The general tendency seen in the reflectance also carries over in

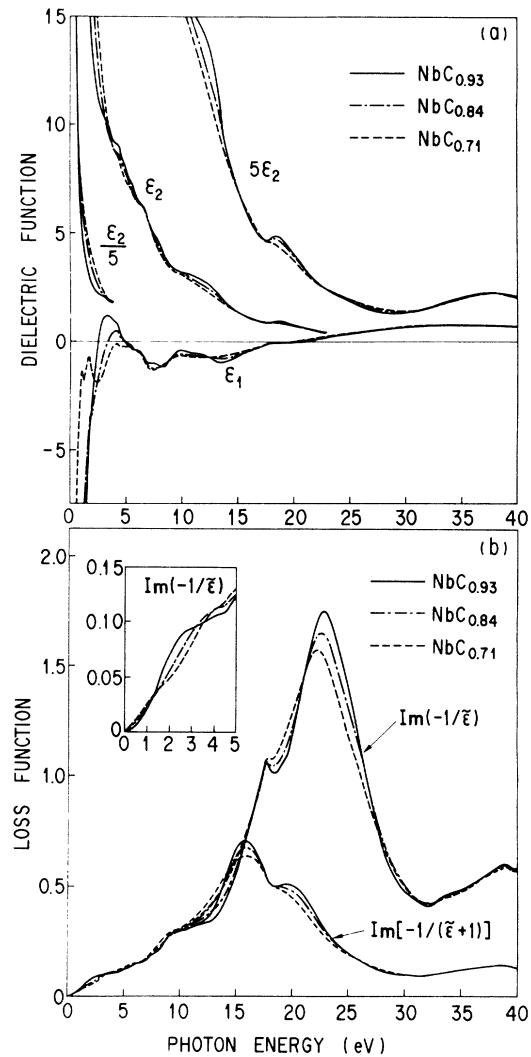


FIG. 9. (a) Real (ϵ_1) and imaginary (ϵ_2) parts of the dielectric function of NbC_x . (b) Electron-energy-loss functions $Im(-1/\epsilon)$ (volume) and $Im[-1/(\epsilon+1)]$ (surface) of NbC_x .

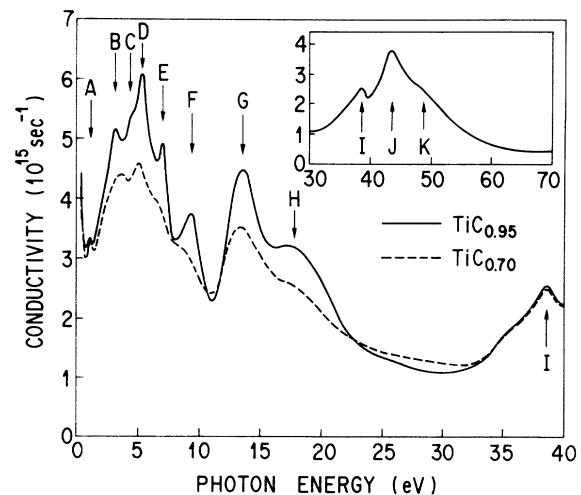


FIG. 10. Optical conductivity of TiC_x . The inset shows the conductivity of $TiC_{0.95}$ in the high-energy region.

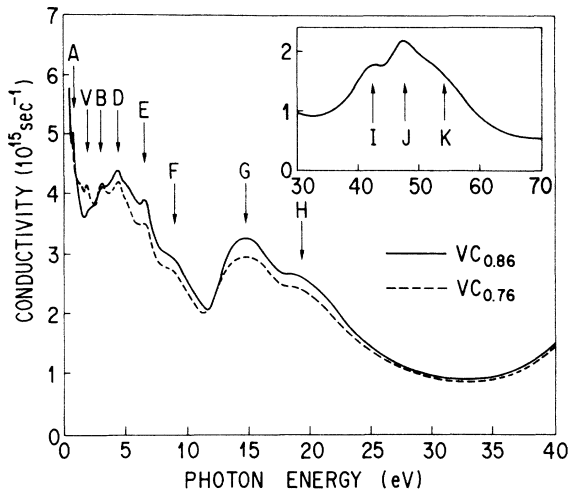


FIG. 11. Optical conductivity of VC_x . The inset shows the conductivity of $VC_{0.86}$ in the high-energy region.

the dielectric function and the conductivity.

The variation of the loss functions with stoichiometry is again most remarkable in TiC_x and far less in NbC_x . Most of the structures below about 10 eV and a peak at ~ 39 eV in TiC_x and NbC_x have counterparts in the ϵ_2 or σ spectrum and are assigned as being due to interband transitions. All of the volume-loss spectra are dominated by the structure centered at 22–24 eV, which can be identified as arising from a volume plasmon. This feature shows a weakening and a shift to lower energy upon decreasing x . A smaller, but well-defined, peak was observed at ~ 11 eV in the volume-loss functions of TiC_x and VC_x , but not in those of NbC_x . This feature lies at a minimum in ϵ_2 and a crossing of the axis by ϵ_1 , with $d\epsilon_1/dE > 0$, and can also be identified as a volume-plasmon structure. The volume-loss spectrum of $NbC_{0.93}$ shows a shoulder at 2.7 eV which is rapidly attenuated as

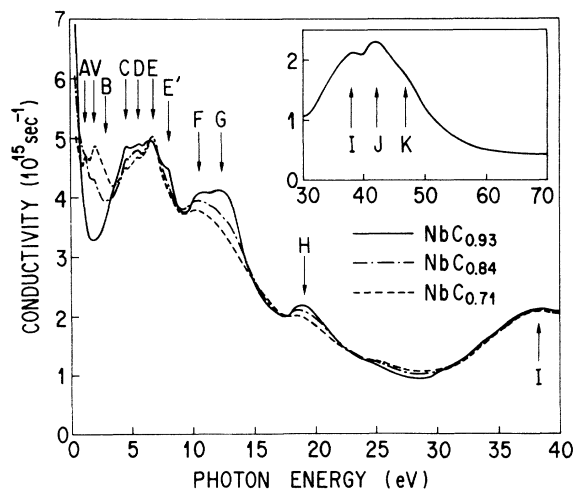


FIG. 12. Optical conductivity of NbC_x . The inset shows the conductivity of $NbC_{0.93}$ in the high-energy region.

the carbon concentration decreases. The surface-loss functions display features which are attributable to surface plasmons. Most of these structures also show a shift to lower energy with damping as the carbon content decreases.

IV. DISCUSSION

We shall consider the results for TiC_x , VC_x , and NbC_x together instead of separately. This allows us to discuss the evolution of the spectra with the metal element as well as with stoichiometry, providing a systematic understanding of the electronic structure of these materials.

A. Interband transitions above 4 eV

The spectra of the near-stoichiometric compounds could be interpreted in terms of the band structure calculated for stoichiometric compounds. The observed interband structures are related to regions of k space, according to the energy separation of the relevant bands, the joint density of states (JDOS), and selection rules which allow or forbid the transitions. Since most of the theoretical studies of vacancy effects indicate that dramatic changes would occur only near the Fermi level,^{62,63,66–69,72–78} the stoichiometry dependence of the features above 4 eV could be reasonably inferred by considering the vacancy effects as the vacancy-induced perturbation on the band structure for $x = 1$.

In Figs. 13 and 14 we reproduce both the energy bands and the partial DOS's of TiC and VC calculated by Neckel *et al.*,⁷ and in Fig. 15 those of NbC obtained by Schwarz.⁸ All of the calculations were made using the self-consistent APW method and the Slater-Koster linear combination of atomic orbitals (LCAO) interpolation scheme. The availability of the partial DOS's will provide an important clue for considering changes with the stoichiometry of the spectral features, as well as in assigning them. Other recent first-principle calculations^{48,53,55} are in good agreement with the bands in Figs. 13–15. However, the results of XPS,^{18,20} UPS,²² and XES (Ref. 39) studies showed that the observed peaks for the occupied bands of carbides and nitrides are, in general, further below E_F than the calculated DOS maxima. Recent ARUPS studies by Weaver *et al.*⁴⁶ and Callenàs *et al.*⁴⁸ for $TiC_{0.93}$ and by Lindberg *et al.* for $VC_{0.80}$ (Ref. 53) and $NbC_{0.83}$ (Ref. 55) have further revealed that the calculations place the filled bands along the Γ - Δ - X line, particularly the Δ_5 and X'_5 states, too close to E_F . Kim and Williams⁸⁴ have carried out a semiempirical band calculation for TiC by incorporating the results of Weaver *et al.*⁴⁶ In the following discussion we refer to such experimental information as well as to the bands in Figs. 13–15 and other calculations.^{48,53,55,84} In Table II, the energies of the features in the present conductivity spectra (Figs. 10–12) are compared with the calculated energies over which interband absorption would be expected.

The partial DOS's show three main maxima: one below E_F (mainly comprising C 2p orbitals with a large amount of metal d components), a lower one above E_F (formed from almost pure metal d orbitals), and an upper

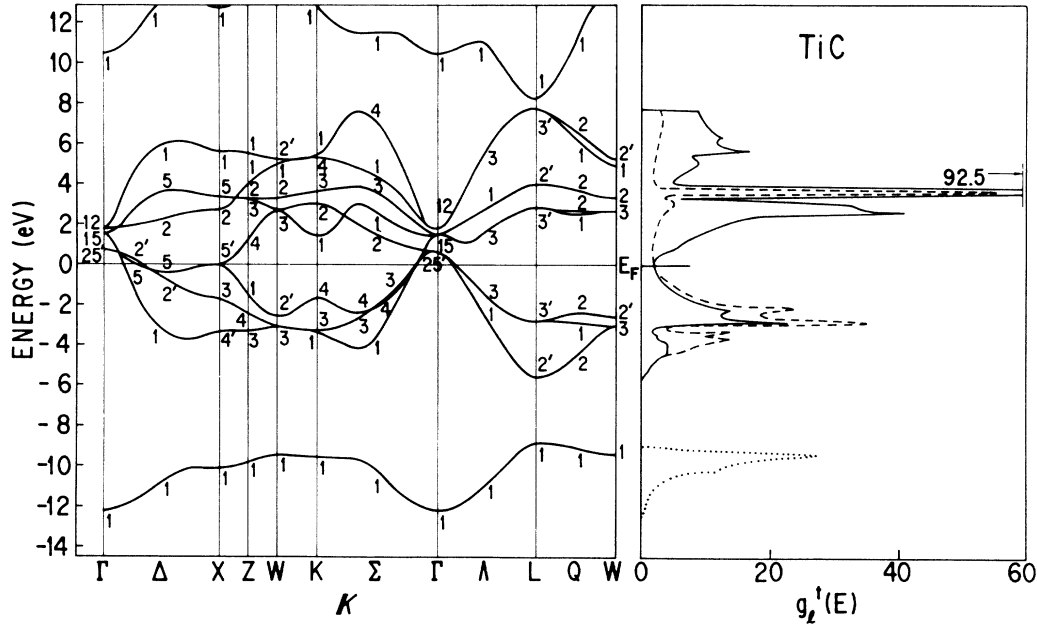


FIG. 13. Energy bands and partial DOS, $g_1'(E)$, for $\text{TiC}_{1.0}$ calculated by Neckel *et al.* (Ref. 7). In the right half, the solid curve represents $g_d^1(E)$, dashed curve $g_p^C(E)$, and dotted curve $g_s^C(E)$. Figure used with permission of the author and publisher of Ref. 7.

one above E_F (primarily containing metal d orbitals with a considerable admixture of C $2p$ character). With the selection rules neglected, one might expect to find strong interband transitions occurring at ~ 5.4 and ~ 6.5 eV in TiC and VC, and ~ 6.3 and ~ 7.2 eV in NbC. Dominant peaks, D and E , do exist in the optical conductivities of three compounds at nearly the same energies, though

there are some differences in energy for D in $\text{VC}_{0.86}$ and for D and E in $\text{NbC}_{0.93}$ (Table II). Similarly, a combination of the lowest and uppermost DOS maxima in the p - d -hybridized bands could give rise to rather strong absorption at ~ 9 eV in TiC and VC and ~ 10.4 eV in NbC. Again, structure F is, in fact, observed in the conductivity spectra at almost the same energies (Table II). With

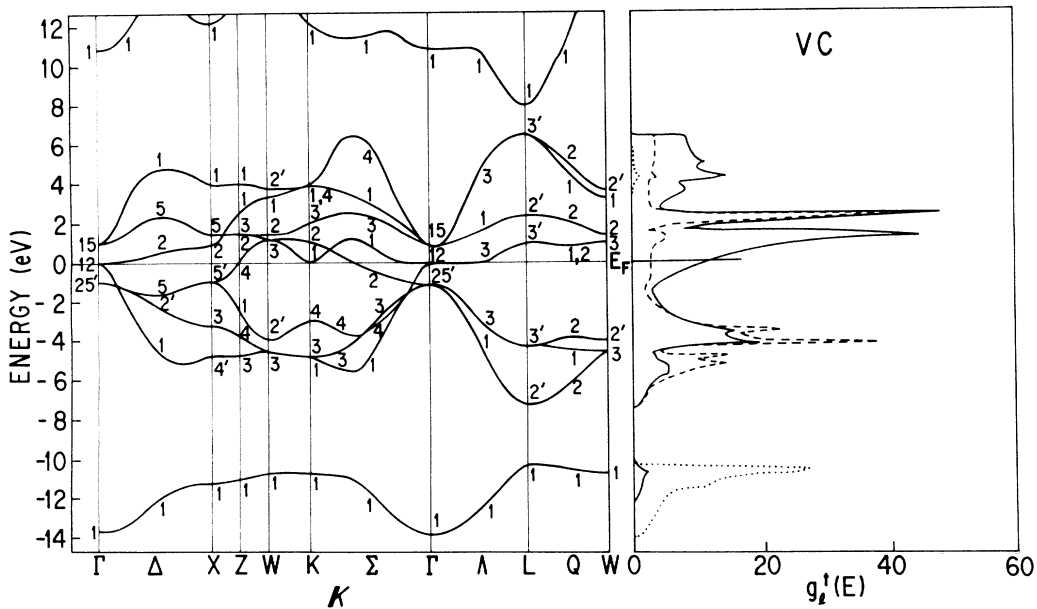


FIG. 14. Energy bands and partial DOS, $g_1'(E)$, for $\text{VC}_{1.0}$ calculated by Neckel *et al.* (Ref. 7). In the right half, the solid curves represent $g_d^V(E)$, dashed curve $g_p^C(E)$, and dotted curves $g_s^C(E)$. Figure used with permission of the author and publisher of Ref. 7.

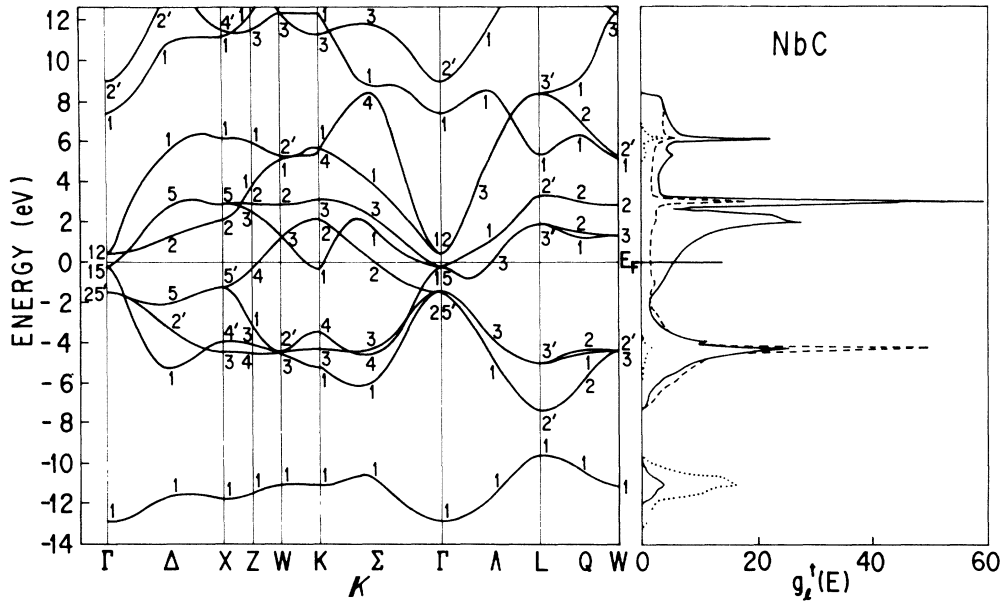


FIG. 15. Energy bands and partial DOS, $g_i^j(E)$, for $\text{NbC}_{1.0}$ calculated by Schwarz (Ref. 8). In the right half, the solid curves represent $g_d^{\text{Nb}}(E)$, dashed curve $g_p^{\text{C}}(E)$, and dotted curves $g_s^{\text{C}}(E)$. Figure used with permission of the author and publisher of Ref. 8.

the selection rules and the band structures taken into account, peak *D* can be identified as arising from transitions between states with a large JDOS lying along the *Q-W* portion of the Brillouin zone, i.e., mainly $Q_2 \rightarrow Q_{1,2}$ and partly $W'_2 \rightarrow W_3$. Peaks *E* and *F* are assigned as being due to transitions between nearly flat bands in the square surface of the Brillouin zone (*X-Z-W-S-U*), with *E* being due to $X'_4 \rightarrow X_5$, $Z_3 \rightarrow Z_{2,3}$, $W_3 \rightarrow W_2$, $S_3 \rightarrow S_{2,3}$, and $U_{1,3} \rightarrow U_{2,3}$, and *F* to $X'_4 \rightarrow X_1$, $Z_3 \rightarrow Z_1$, $W_3 \rightarrow W'_2$, $S_3 \rightarrow S_1$, and $U_{1,3} \rightarrow U_{1,4}$. The regions of *k* space near *X* probably make a dominant contribution. The reason why peaks *D* and *E* in $\text{TiC}_{0.95}$ are sharper than those in $\text{NbC}_{0.93}$ could be that the states satisfying the selection rules for the allowed transitions coincide in energy with the DOS maxima for TiC, whereas there are some differences for NbC. The situations for VC look similar to those for TiC.

Feature *E'* in NbC_x has no counterpart in TiC_x and VC_x and exhibits a very rapid loss in intensity upon going from $x=0.93$ to 0.84. A comparison of the band structure of NbC with those of TiC and VC shows that $\Gamma_{15} \rightarrow \Gamma_1$ absorption can take place in NbC with an energy appropriate for *E'* but not in TiC and VC, since the Γ_{15} level is filled in NbC but empty in TiC and VC. We thus attribute *E'* in $\text{NbC}_{0.93}$ to the $\Gamma_{15} \rightarrow \Gamma_1$ transition. If this assignment is correct, its *x*-dependent behavior indicates that the Fermi level moves downward in NbC_x , crossing the Γ_{15} level as *x* is lowered from 0.93 to 0.84. Further evidence is given later for the shift of E_F to lower energy. From the bands in Figs. 13–15 alone, there seems to be no suitable candidates for a transition responsible for feature *C* in $\text{TiC}_{0.95}$ and NbC_x . However, by taking into account the results of ARUPS studies,^{46,48,53–56,59} we can reasonably identify shoulder *C* in $\text{TiC}_{0.95}$ as being

due to the $\Delta_5 \rightarrow \Delta_5$ transition near *X* and peak *C* in NbC_x to the $X'_5 \rightarrow X_5$ and $\Delta_5 \rightarrow \Delta_5$ (near *X*) transitions. Since the initial states are located in a low-DOS region, but the final states lie at a main DOS maximum, an appreciable intensity is expected to result. For VC, the energy separation of the associated bands is too small to produce any structure at this energy, even though the results of ARUPS studies^{53,54} are considered. Those transitions may overlap the lower-lying structure, *B*.

The band structures as well as the DOS's predict that strong absorption within the *p-d*-hybridized bands will be exhausted at about 11 eV and transitions to the higher metal-*s* band will start at 11–12 eV. For TiC and VC, a small energy gap exists between the metal *s* and *d* bands, which would give rise to a deep dip at ~ 11 eV in the measured spectra. In contrast, for NbC, there is an appreciable overlap of the metal *s* and *d* bands, which could result in a much shallower minimum in the experimental spectra. A combination of the C 2*s* DOS peak and the main DOS maximum above E_F containing a large amount of the C 2*p* component could lead to a transition from the C 2*s* to *d* bands occurring at ~ 13 eV in TiC, ~ 12.7 eV in VC, and ~ 14 eV in NbC. The experimental optical conductivities have been found to exhibit the corresponding feature, *G*. It is located at energies ~ 0.6 and ~ 2 eV larger than the calculations in $\text{TiC}_{0.95}$ and $\text{VC}_{0.86}$, respectively. For $\text{NbC}_{0.93}$, the proximity of feature *F* prevents an exact determination of its position in the conductivity, although the reflectance shows *G* at nearly the same energy expected from the calculations. Structure *H* would arise from transitions with a large JDOS between the *p-d*-hybridized bands below E_F and the higher-lying bands.

A comparison of the observed energies of interband

TABLE II. Energies of features observed in the present conductivity spectra of TiC_x , VC_x , and NbC_x and calculated energies over which interband absorption would be expected. The energy of states belonging to D_i representation, $E(D_i)$, is abbreviated as D_i . All energies are given in eV.

	A	V	B	C	D	E	E'	F	G	H
TiC_x	1.15 1.16		3.2 ~3.7	~4.5	5.4 5.1	7.0 ~6.7		9.3 ~9.0	13.6 13.3	~17.2 ~17
$\text{TiC}_{1.0}$	$\Lambda_3 - \Lambda_3 = 1.2$		$\left[\begin{array}{l} K_1 - K_4 = 3.1 \\ X_2 - X'_5 = 2.7 \\ \Delta_2 - \Delta_5 = \sim 2.7 \end{array} \right]$	$\Delta_5 - \Delta_5 = 3.4-4$ ($X_5 - X'_5 = 3.3$)	$Q_{1,2} - Q_2 = 4.9-5.1$ $W_3 - W'_2 = 5.2$	$X_5 - X'_4 = 6.7$ $Z_{2,3} - Z_3 = 6.5$ $W_2 - W_3 = 6.4$		$X_1 - X'_4 = 8.9$ $Z_1 - Z_3 = 8.8$ $W'_2 - W_3 = 8.3$		
Kim and Williams ^c	$\Lambda_3 - \Lambda_3 = 0.85$		$\left[\begin{array}{l} X_2 - X'_5 = 3.3 \\ \Delta_2 - \Delta_5 = \sim 3.4 \end{array} \right]$	$\Delta_5 - \Delta_5 = 4-5$ ($X_5 - X'_5 = 4.0$)	$Q_{1,2} - Q_2 = 5.3-5.6$ $W_3 - W'_2 = 5.5$	$X_5 - X'_4 = 7.8$ $Z_{2,3} - Z_3 = 7.7$ $W_2 - W_3 = 7.6$		$X_1 - X'_4 = 10.1$ $Z_1 - Z_3 = 9.7$ $W'_2 - W_3 = 9.3$		
Callenás et al. ^d	$\Lambda_3 - \Lambda_3 = 1.1$		$\left[\begin{array}{l} K_1 - K_4 = 3.2 \\ X_2 - X'_5 = 2.9 \\ \Delta_2 - \Delta_5 = \sim 3 \end{array} \right]$	$\Delta_5 - \Delta_5 = 3.5-4.1$ ($X_5 - X'_5 = 3.5$)		$X_5 - X'_4 = 6.8$ $S_3 - S_3 = 6.8$ $U_5 - U_{1,3} = 6.8$		$X_1 - X'_4 = 9.1$ $S_1 - S_3 = 9.0$ $U_{1,4} - U_{1,3} = 8.8$		
VC_x	0.7	~1.95 1.85	~3.1 3.1		4.4 4.4	6.5 6.4		~9.0 ~8.8	14.7 ~14.6	~19 ~19
$\text{VC}_{1.0}$	$\Gamma_{15} - \Gamma_{12} = 0.85$		$\left[\begin{array}{l} K_1 - K_4 = 3.0 \\ \Gamma_{15} - \Gamma'_{25} = 1.95 \\ \Sigma_3 - \Sigma_2 = 2-2.6 \\ X_2 - X'_5 = 1.9 \\ \Delta_2 - \Delta_5 = 2.1 \end{array} \right]$		$Q_{1,2} - Q_2 = 4.5$	$X_5 - X'_4 = 6.2$ $Z_{2,3} - Z_3 = 6.2$ $W_2 - Z_3 = 5.9$		$X_1 - X'_4 = 8.7$ $Z_1 - Z_3 = \sim 8.7$ $W'_2 - W_3 = 9.3$		
Lindberg et al. ^c	$\Gamma_{15} - \Gamma_{12} = 1$ $\Delta_5 - \Delta_2 = \sim 1$		$\left[\begin{array}{l} K_1 - K_4 = 3.2 \\ \Gamma_{15} - \Gamma'_{25} = 1.9 \\ \Sigma_3 - \Sigma_2 = 1.9-2.3 \\ X_2 - X'_5 = 2.0 \\ \Delta_2 - \Delta_5 = \sim 2.1 \end{array} \right]$			$X_5 - X'_4 = 6.7$ $Z_{2,3} - Z_3 = \sim 6.7$ $W_2 - W_3 = 6.5$ $S_{2,3} - S_3 = 6.4-6.8$		$X_1 - X'_4 = 9.3$ $Z_1 - Z_3 = \sim 9.1$ $S_1 - S_3 = 9.2$ $U_{1,4} - U_{1,3} = 9.1$ $W'_2 - W_3 = 8.5$		
NbC_x		~1.9 1.9	(~3)	4.5 4.5 4.45	5.6 5.5 5.4	6.6 6.75 6.7	8.0 (~7.8)	10.7 10.4 10.2	~13	18.8 18.6 18.4
$\text{NbC}_{0.93}$ $\text{NbC}_{0.84}$ $\text{NbC}_{0.71}$										
$\text{NbC}_{1.0}$	$\Gamma_{15} - \Gamma'_{25} = 1.2$		$\left[\begin{array}{l} K_1 - K_4 = 3.1 \\ X_2 - X'_5 = 3.2 \\ \Delta_2 - \Delta_5 = 3.2-3.3 \end{array} \right]$	$X_5 - X'_5 = 4.1$ $\Delta_5 - \Delta_5 = 4.1-5$	$Q_{1,2} - Q_2 = 5.4-5.8$ $W_3 - W'_2 = 5.6$	$X_5 - X'_4 = 6.7$ $Z_{2,3} - Z_3 = 6.6-6.9$ $W_2 - W_3 = 7.2$	$\Gamma_1 - \Gamma_{15} = 7.6$	$X_1 - X'_4 = 10.0$ $Z_1 - Z_3 = 9.9$ $W'_2 - W_3 = 9.7$		
Lindberg et al. ^f	$\Gamma_{15} - \Gamma'_{25} = 1.2$		$\left[\begin{array}{l} K_1 - K_4 = 3.3 \\ X_2 - X'_5 = 2.9 \\ \Delta_2 - \Delta_5 = \sim 2.9 \end{array} \right]$	$X_5 - X'_5 = 4.3$ $\Delta_5 - \Delta_5 = 4.2-4.9$	$W_3 - W'_2 = 5.8$	$X_5 - X'_4 = 6.8$ $Z_{2,3} - Z_3 = 6.9-7$ $S_{2,3} - S_3 = 6.8$ $U_2 - U_3 = 6.5$	$\Gamma_1 - \Gamma_{15} = 8.4$	$X_1 - X'_4 = 10.0$ $Z_1 - Z_3 = 10.0$ $W'_2 - W_3 = 9.9$		

^dReference 48.

^cReference 53.

^fReference 55.

structures, $C-G$, with those expected from the first-principles calculations^{7,8,48,53,55} shows that the calculations generally give smaller energy separations, which is consistent with the energies for the occupied bands determined from UPS (Ref. 22) and ARUPS (Refs. 46, 48, 53, and 55) experiments. The semiempirical calculation for TiC by Kim and Williams⁸⁴ seems to slightly overestimate the correction from the ARUPS results of Weaver *et al.*⁴⁶

All of the structures between 4 and 20 eV exhibit a decreasing intensity with lowering x , except for the main peak, E , in NbC_x . This is naturally expected from a concomitant reduction in the available C $2p$ and C $2s$ orbitals and is also in agreement with the results of calculations for the stoichiometry-dependent partial DOS.^{62–78} Structure E in TiC_x and VC_x shows an intensity decrease much larger than structure D . This behavior could be understood in terms of the orbital nature of the associated bands. We have assigned D as being due to a transition involving a final state formed from almost pure d orbitals and E to a transition related with the d -like state with considerable admixture of p character. The ratio of the p and d components in the initial state is nearly the same for both transitions. The decreased carbon content leads to reduced effective p - d hybridization. This could cause changes in the transition matrix elements, presumably a reduction, which would result in a larger decrease in the strength of E more than that of D . By considering that the bands of NbC have less p - d hybridization than those of TiC and VC (Figs. 13–15), the same argument could be applied to account for the fact that x -dependent changes in the strength of the features above 4 eV are smaller in NbC_x than in TiC_x and VC_x .

The p - d hybridization could also be related to the peak shifts with stoichiometry. The p - d mixing will cause the repulsion of the hybridized bonding and antibonding states. The reduced p - d hybridization would effectively reduce the repulsion of those states, resulting in a shift to lower energy of the associated transition energies. Further, the smaller p - d mixing in NbC could account for the smaller energy shifts in NbC_x than in TiC_x .

It seems to be puzzling at first sight that structure E in NbC_x remains almost unchanged in peak height and shows a sharpening rather than a broadening as the carbon concentration decreases. Marksteiner *et al.*⁷³ have recently calculated the carbon-content-dependent partial DOS for $3d$ - and $4d$ -metal carbides and nitrides using the Korringa-Kohn-Rostoker coherent-potential-approximation (KKR-CPA) method. Their results show that the Ti $4p$ or V $4p$ state makes only a small contribution to the p -band DOS, but that the Nb $5p$ state shows a considerably larger contribution (not shown in Fig. 15). Because the Nb $5p \rightarrow \text{Nb } 4d$ absorption takes place on site, its dipole matrix element would be larger than that of the C $2p \rightarrow \text{Nb } 4d$ charge-transfer transition. This could partly account for the insensitivity of the strength of E to changes in the carbon content. Later we describe a more essential contribution of the metal p state to the optical spectra. The transitions responsible for peak E occur over wide regions of \mathbf{k} space with slightly different energies (Table II). The loss of carbon may give rise to a

more rapid loss of transitions involving states with a larger amount of the C $2p$ component, resulting in a sharpening of E . The nonmonotonic energy shift of E with stoichiometry (Table II) might also originate from its complicated structure.

B. Transitions below 4 eV with marked stoichiometry dependence

The structures below 4 eV, which exhibit a dramatic stoichiometry dependence in VC_x and NbC_x , should be interpreted on the basis of calculations which make a full treatment of the vacancy effects. Though an APW band-structure calculation has been performed for $\text{TiC}_{0.75}$ with completely ordered vacancies,⁶⁶ no such calculations are available for VC_x and NbC_x . Nevertheless, some aspects of the observed features can be well explained in terms of the band structures for $x=1$ (Figs. 13–15) together with the x -dependent partial-DOS calculations.^{66,68,69,73,74,76–78}

The lowest-lying feature, A , should be associated with transitions between states near E_F . Peak A in TiC_x can be identified as originating from an initial state at E_F near the center of the Brillouin zone, i.e., $\Lambda_3 \rightarrow \Lambda_3$. A shift of E_F would lead to a shift in energy of such a transition, but that is not the case (Table II). This might be due to the nearly parallel dispersion of the initial- and final-state bands. Feature A in $\text{VC}_{0.86}$ is attributable to the $\Gamma_{12} \rightarrow \Gamma_{15}$ transition. Since the Γ_{12} level is touching E_F in Fig. 14 (or just below E_F in the bands of Lindberg *et al.*⁵³), a loss of peak A in $\text{VC}_{0.76}$ shows that the Fermi level moves downward as x decreases, with E_F crossing Γ_{12} between $x=0.86$ and 0.76 . In contrast, feature A appears in NbC_x upon lowering x . This can be well understood by identifying A as arising from a transition from the $\Gamma_{25'} \rightarrow \Gamma_{15}$ states, with Γ_{15} becoming vacant due to a downward shift of E_F upon decreasing x . It is also possible for the $\Gamma_{15} \rightarrow \Gamma_{12}$ transition to generate another feature on the low-energy side of A and disappear as x decreases. There is a sign of the associated feature in $\text{NbC}_{0.93}$ spectrum (Fig. 12), though it is not distinctly discernible because the transition falls around the lower-energy limit of the present measurements. This assignment of A and its x -dependent behavior are completely consistent with the identification of E' as being due to the $\Gamma_{15} \rightarrow \Gamma_1$ transition.

With the results of the ARUPS studies^{46,48,53,54} considered, the $X'_5 \rightarrow X_2$ and $\Delta_5 \rightarrow \Delta_2$ (near X) transitions may be responsible for peak B in TiC_x and VC_x . For VC_x , the $\Gamma_{25'} \rightarrow \Gamma_{15}$ and $\Sigma_2 \rightarrow \Sigma_3$ (near Γ) transitions may also give rise to B . However, we rule out their main contribution to B for the following reasons. First, a feature due to the $X'_5 \rightarrow X_2$ or $\Delta_5 \rightarrow \Delta_2$ absorption should be observed in NbC as well at almost the same energy, which contradicts the experimental result for $\text{NbC}_{0.93}$ (Fig. 12). Second, peak B in TiC_x is much stronger than feature C assigned as being due to the $\Delta_5 \rightarrow \Delta_5$ transition, which is in conflict with the calculated result that the Δ_5 final state has a much higher DOS than the Δ_2 state does (Fig. 13).

Finally, the intensity increase of B in VC_x with lowering x is difficult to explain in terms of the $\Gamma_{25'} \rightarrow \Gamma_{15}$ and $\Sigma_2 \rightarrow \Sigma_3$ transitions, since those final states consist primarily of the C $2p$ orbital. Thus, we propose another identification of B as arising from the $K_4 \rightarrow K_1$ transition, which can account for all of the observed behavior of B . It should be noted that the K_1 level is located well above E_F in TiC (i.e., vacant), is nearly touching E_F in VC (i.e., nearly vacant), and is just below E_F in NbC (i.e., filled) (Figs. 13–15). In conjunction with the observed downward shift of E_F with decreasing x , this gives a reasonable explanation for the observations that peak B is present irrespective of x in TiC_x , gains strength with lowering x in VC_x , and is not seen in $NbC_{0.93}$ and $NbC_{0.84}$ with its faint signature appearing in $NbC_{0.71}$. These results show that the Fermi level crosses the K_1 state upon going from $x=0.86$ to 0.76 in VC_x and nearly touches the K_1 level in $NbC_{0.71}$. By using the present result for NbC_x and assuming that the calculated band structure for NbC places the K_1 state at the correct energy with respect to E_F , we can estimate a shift of E_F to be $|\Delta E_F| = 0.25\text{--}0.3$ eV between $x=1$ and 0.71 . The KKR-CPA calculation by Marksteiner *et al.*⁷³ gives $|\Delta E_F| = 0.76$ eV, which is a factor of ~ 3 larger than the present result.

Feature V in VC_x and NbC_x cannot be interpreted at all in terms of the band structure for $x=1$; there are no possible bands satisfying the selection rules with an appropriate energy separation and its marked gain in strength with lowering x is more difficult to explain. Many of the recent theoretical treatments of the vacancy effects^{62,63,66–69,72–78} predict new vacancy-induced states near E_F , formed from symmetric combinations of the electronic states of surrounding atoms. Among them, the KKR-CPA results⁷³ show that vacancy states having a_{1g} and t_{1u} symmetries with respect to the vacant site appear below E_F in nonstoichiometric carbides and nitrides. Their results also show that those states shift to higher energies upon lowering x , and that the t_{1u} state is considerably broad with an appreciable DOS above E_F at low x . The XPS (Ref. 17) and ARUPS (Refs. 54–56 and 59) studies have revealed the presence of a filled vacancy state about 2 eV below E_F for VC_x and NbC_x . In particular, the ARUPS spectra for $VC_{0.80}$ of Lindberg *et al.*⁵⁴ showed a vacancy-induced peak which is in good agreement with the a_{1g} -symmetry DOS peak predicted from the KKR-CPA calculations.⁷³ With these recent theoretical and experimental results, we can reasonably attribute feature V in VC_x and NbC_x to a transition from an a_{1g} vacancy state below E_F to part of a t_{1u} vacancy state just above E_F . This assignment of V gives a reasonable explanation for its remarkable intensity increase with decreasing x . Although no direct observation has yet been reported of an unoccupied portion of a t_{1u} vacancy state, the present result indicates its presence. The observed downward shift of E_F with decreasing x suggests that vacancy states formed below E_F accommodate excess electrons released from the carbon vacancies.

We note here two interesting aspects of vacancy-induced feature V : (1) The structure in NbC_x is much

more intense than that in VC_x ; (2) no counterpart is discernible in TiC_x . An explanation is required for (1), since a vacancy peak observed in ARUPS studies^{54–56} shows a comparable strength for $VC_{0.80}$ and $NbC_{0.83}$. Our result (2) is consistent with no evidence for a shift of peak A and in agreement with that of Lynch *et al.*;²⁹ their spectra for TiC_x exhibit only very small changes with stoichiometry in the low-energy region. Neither UPS (Ref. 22) nor ARUPS (Refs. 46, 48, and 52) studies have also detected any vacancy peak in TiC_x and ZrC_x . However, these observations seem to contradict the fact that a vacancy-related feature was detected for TiC_x in earlier XPS (Ref. 16) (identified recently by Redinger *et al.*⁷⁴) and XES (Ref. 38) spectra. In order to explain both (1) and (2), we shall consider two factors: (a) the degree of metal p contribution to the vacancy DOS; (b) the location of the lower a_{1g} -symmetry vacancy state with respect to E_F . Most of the interpretations of vacancy states have been made by taking into account the metal d contribution alone, because the calculated metal p partial DOS was very small. However, recent XPS, UPS, and XES studies by Mariot *et al.*^{20,39,40} and XPS intensity calculations by Redinger *et al.*⁷⁴ have shown that the metal p state plays an important role in the interpretation of XPS spectra through the cross-section effects. The metal p contribution would be more essential for the present optical spectra, since optical absorption from an a_{1g} - to a t_{1u} -symmetry vacancy state will be dominated by an intra-atomic transition between the energy-shifted metal p and e_g states. The KKR-CPA results^{73,74} show that the Nb $5p$ orbital contributes appreciably to the local vacancy DOS as well as to the intrinsic p -band DOS, whereas the contributions of the Ti and V $4p$ orbitals are small. This leads to a reasonable explanation of (1). The Fermi level in TiC_x and ZrC_x is lower than that in other carbides and nitrides, resulting in the proximity of the a_{1g} -symmetry vacancy state to E_F ; the state is located only 0.4 eV below E_F in an APW calculation for $TiC_{0.75}$;⁶⁶ most of the vacancy-induced states in TiC_x and ZrC_x are above E_F in the KKR-CPA calculations.^{73,74} In fact, a vacancy-induced feature observed in XPS (Ref. 16) and XES (Ref. 38) spectra is located just below E_F . This proximity to E_F would result in the loss of transition intensities associated with the a_{1g} vacancy state. Therefore, consideration of both (a) and (b) can account well for our result (2). The failure of UPS (Ref. 22) and ARUPS (Refs. 46, 48, and 52) studies to detect a vacancy state in either TiC_x or ZrC_x can also be understood by (a) and (b) together with the cross-section effects.

C. Plasmon structures

The energies of the structures in the loss functions are given in Table III together with those reported in the literature.^{29,44} The energy of the main volume plasmon could be compared to the free-electron-gas plasmon energy given by

$$E_p = \hbar e \left(\frac{4\pi N}{m V_a} \right)^{1/2}, \quad (2)$$

TABLE III. Loss functions and plasmon parameters in TiC_x , VC_x , and NbC_x . All energies in eV. A blank means no data available.

	TiC_x		VC_x		NbC_x		
	$\text{TiC}_{0.95}$	$\text{TiC}_{0.70}$	$\text{VC}_{0.86}$	$\text{VC}_{0.76}$	$\text{NbC}_{0.93}$	$\text{NbC}_{0.84}$	$\text{NbC}_{0.71}$
Present work	high-energy peak in $\text{Im}(-1/\tilde{\epsilon})$	23.3	21.9	24.6	24.1	22.8	22.6
	low-energy peak in $\text{Im}(-1/\tilde{\epsilon})$	11.1	10.8	11.6	11.3		
	Drude plasmon loss in $\text{Im}(-1/\tilde{\epsilon})$					2.7	
	high-energy peak in $\text{Im}[-1/(\tilde{\epsilon}+1)]$	20.3	(~19.5)	20.6	(~20.2)	19.7	(~19.5)
low-energy peak in $\text{Im}[-1/(\tilde{\epsilon}+1)]$	10.7	10.2	10.8	10.5	15.8	15.8	15.8
Calculated							
	free-electron E_p	23.0	21.6	25.3	24.9	23.3	22.9
	$E_p/\sqrt{2}$	16.3	15.2	17.9	17.6	16.5	16.2
From previous optical data ^a							
	high-energy peak in $\text{Im}(-1/\tilde{\epsilon})$	22.6	21.1				
		($x=0.90$)	($x=0.64$)				
	low-energy peak in $\text{Im}(-1/\tilde{\epsilon})$	11.2	~10.8				
		($x=0.90$)	($x=0.64$)				
	high-energy peak in $\text{Im}[-1/(\tilde{\epsilon}+1)]$	~20					
		($x=0.90$)					
	low-energy peak in $\text{Im}[-1/(\tilde{\epsilon}+1)]$	~10.4	~9.8				
		($x=0.90$)	($x=0.64$)				
From ELS measurements ^b							
	electron-energy loss near E_p	23.5	23.2	24.9	24.6	24.0	
		($x=1.0$)	($x=0.7$)	($x=0.88$)	($x=0.78$)	($x=1.0$)	
	low-energy electron-energy loss	11.4	~11.3	11.9	~11.8		
		($x=1.0$)	($x=0.7$)	($x=0.88$)	($x=0.78$)		
	Drude plasmon loss					2.9	
						($x=1.0$)	

^aReference 29.^bReference 44.

where e is the electron charge, m the free-electron mass, N the number of valence electrons per unit cell, and V_a the unit-cell volume. By taking into account the metal $3d$ and $4s$ (or $4d$ and $5s$) electrons as well as the carbon $2s$ and $2p$ electrons as the valence electrons, we calculated the values of E_p (Table III). The calculated energies are found to be in good agreement with the experimental values. However, a closer examination of the observed energies shows that their x -dependent shift in NbC_x is about a factor of 2 smaller than that expected from the nominal decrease in the number of valence electrons due to carbon vacancies and from an application of Eq. (2); in contrast, agreement is good for TiC_x and VC_x . Lynch *et al.*²⁹ obtained a shift with stoichiometry for TiC_x which is also in good agreement with the calculated value. From the ELS spectra, Pflüger *et al.*⁴⁴ found the main volume plasmon at energies close to the free-electron-gas plasmon in $3d$ transition-metal carbides and nitrides with and without nonmetal vacancies. Their peak shifts with stoichiometry were found to be less than one would expect from Eq. (2) for all compounds. In particular, the observed shift in TiC_x was -0.3 eV from $x=1$ to 0.7, much smaller than the calculated value of -1.7 eV. In this respect, there are discrepancies between the results from optical measurements and ELS measurements. This might be partly due to the difference in sample preparation; our samples and that of Lynch *et al.*²⁹ ($x=0.90$) are single crystals, while those of Pflüger *et al.*⁴⁴ are thin films prepared by reactive sputtering.

The 2.7-eV feature in the volume-loss spectrum of $\text{NbC}_{0.93}$ lies at a zero crossing in ϵ_1 curve. The structure was previously reported in the loss spectrum of Pflüger *et al.* for $\text{NbC}_{1.0}$,⁴⁴ slightly sharper than in ours. The counterpart was also observed for TiN_x and VN_x by them⁴⁴ and for VN_x , ZrN_x , and NbN_x by Schubert *et al.*²³ It should be noted that these nitrides show very weak interband transitions below ~ 3 eV. Pflüger *et al.*⁴⁴ identified the very sharp peak in TiN_x as arising from the Drude plasmon excitation shifted down by interband transitions at higher energies. They accounted for its absence in TiC_x as being due to a larger damping caused by appreciable low-energy interband effects. The same argument would be applicable to the present 2.7-eV feature. In fact, the low-energy extrapolation process for the Kramers-Kronig analysis showed that the low-energy reflectance of NbC_x could be best approximated by the Drude-like treatment among the present samples. Furthermore, the damping constant of the free-electron gas determined by the fitting displayed a remarkable enhancement with decreasing x , indicating increased scattering due to carbon vacancies. Thus, we can reasonably interpret the 2.7-eV feature as being due to the screened Drude plasmon, with its rapid attenuation arising from the influence of carbon vacancies. A closer examination of the spectra shows that the feature seems to shift to higher energy upon lowering x [Fig. 9(b)]; this could be seen more evidently as a shift in the zero crossing in ϵ_1 [Fig. 9(a)]. This behavior can be well understood by the reduced interband effects at higher energies with decreasing x .

The surface-loss function of $\text{TiC}_{0.95}$ shows two well-defined peaks, one at 20.3 eV and the other at 10.7 eV. Corresponding structures are less distinctly visible in $\text{TiC}_{0.70}$ and VC_x , and the higher one also in NbC_x . None of them are located at energies predicted by the free-electron-gas $1/\sqrt{2}$ relation of surface to bulk-plasmon energy (Table III). In contrast, the main surface-loss peak in NbC_x (~ 16 eV) can be related to the main volume-plasmon peak by a factor of $\sqrt{2}$. Unlike other plasmon structures, it shows no appreciable energy shift with stoichiometry.

V. CONCLUSIONS

The optical properties of TiC_x , VC_x , and NbC_x have been systematically studied to supply new, detailed information about how the vacancies modify the electronic structure. The spectra of VC_x and NbC_x below 4 eV showed dramatic variations with stoichiometry, whereas those of TiC_x exhibited only small changes. Above 4 eV, in contrast, the spectra of TiC_x displayed the most distinct dependence on the carbon concentration.

With the reported partial DOS (Refs. 7 and 8) and information from recent ARUPS studies^{46,48,53,55} taken into account, many of the observed interband structures could be identified in the band structures previously calculated for $x=1$.^{7,8,48,53,55,84} The characteristic difference in the energy shifts and intensity changes of the main peaks above 4 eV was interpreted in terms of the difference in the degree of p - d hybridization. Some of the features below 4 eV in VC_x and NbC_x , which appear, disappear, or remarkably changes in strength upon decreasing x , could be assigned as being due to transitions involving initial or final states near the Fermi level. This led to the conclusion that the Fermi level moves downward with lowering x in VC_x and NbC_x . A feature which markedly gains strength as x decreases was observed at ~ 2 eV for VC_x and NbC_x , whereas no counterpart was seen for TiC_x . This structure cannot be identified in the band structures for $x=1$ and was attributed to a transition between vacancy-induced states located below and immediately above the Fermi level. Its marked strength in NbC_x was explained as the result of an appreciable metal- p -state contribution to the vacancy states. The present optical observation of a vacancy-induced feature indicates the presence of not only an occupied a_{1g} -symmetry vacancy state, but also an unoccupied portion of a t_{1u} -symmetry vacancy state, the latter of which has been predicted theoretically but not observed experimentally.

The main volume-plasmon energies were favorably compared to the free-electron plasmon energies, though disagreement was found in NbC_x for the energy shift with stoichiometry. The Drude plasmon structure was observed in NbC_x , reflecting the fact that the low-energy spectra of NbC_x most resemble the Drude-like behavior among the compounds studied. Its rapid attenuation with decreasing x indicates the increased scattering due to defects.

ACKNOWLEDGMENTS

We thank the staff of the Photon Factory, National Laboratory for High Energy Physics, for their support,

and Y. Anahara of Production Engineering Research Laboratory, Canon, Inc. for his help in measuring the surface roughness of the samples.

- ¹L. E. Toth, *Transition Metal Carbides and Nitrides* (Academic, New York, 1971).
- ²E. K. Storms, *The Refractory Carbides* (Academic, New York, 1967).
- ³H. Bilz, *Z. Phys.* **153**, 338 (1958).
- ⁴J.-L. Calais, *Adv. Phys.* **26**, 847 (1977).
- ⁵A. Neckel, *Int. J. Quantum Chem.* **23**, 1317 (1983).
- ⁶K. Schwarz, *CRC Crit. Rev. Solid State Mater. Sci.* **13**, 211 (1987).
- ⁷A. Neckel, P. Rastl, R. Eibler, P. Weinberger, and K. Schwarz, *J. Phys. C* **9**, 579 (1976).
- ⁸K. Schwarz, *J. Phys. C* **10**, 195 (1977).
- ⁹K. Schwarz, H. Ripplinger, and A. Neckel, *Z. Phys. B* **48**, 79 (1982).
- ¹⁰D. A. Papaconstantopoulos, W. E. Pickett, B. M. Klein, and L. L. Boyer, *Phys. Rev. B* **31**, 752 (1985).
- ¹¹P. Blaha and K. Schwarz, *Int. J. Quantum Chem.* **23**, 1535 (1983).
- ¹²P. Blaha, J. Redinger, and K. Schwarz, *Phys. Rev. B* **31**, 2316 (1985).
- ¹³P. Blaha and K. Schwarz, *Phys. Rev. B* **36**, 1420 (1987).
- ¹⁴Band-structure calculations for stoichiometric compounds using the LAPW method are also given in Refs. 47–49, 52, 53, 55, and 58.
- ¹⁵H. Ihara, Y. Kumashiro, and A. Itoh, *Phys. Rev. B* **12**, 5465 (1975); H. Ihara, M. Hirabayashi, and H. Nakagawa, *ibid.* **14**, 1707 (1976), and references therein.
- ¹⁶L. I. Johansson, A. L. Hagström, B. E. Jacobson, and S. B. M. Hagström, *J. Electron Spectrosc. Relat. Phenom.* **10**, 259 (1977); A. L. Hagström, L. I. Johansson, S. B. M. Hagström, and A. N. Christensen, *ibid.* **11**, 75 (1977).
- ¹⁷H. Höchst, P. Steiner, S. Hüfner, and C. Politis, *Z. Phys. B* **37**, 27 (1980), and references therein.
- ¹⁸L. Porte, L. Roux, and J. Hanus, *Phys. Rev. B* **28**, 3214 (1983); L. Porte, *Solid State Commun.* **50**, 303 (1984).
- ¹⁹G. R. Gruzalski and D. M. Zehner, *Phys. Rev. B* **34**, 3841 (1986).
- ²⁰G. Indlekofer, J.-M. Mariot, W. Lengauer, E. Beauprez, P. Oelhafen, and C. F. Hague, *Solid State Commun.* **72**, 419 (1989).
- ²¹L. I. Johansson, P. M. Stefan, M. L. Shek, and A. N. Christensen, *Phys. Rev. B* **22**, 1032 (1980), and references therein.
- ²²J. H. Weaver and F. A. Schmidt, *Phys. Lett. A* **77**, 73 (1980).
- ²³W. K. Schubert, R. N. Shelton, and E. L. Wolf, *Phys. Rev. B* **23**, 5097 (1981); **24**, 6278 (1981).
- ²⁴H. Höchst, R. D. Bringans, P. Steiner, and Th. Wolf, *Phys. Rev. B* **25**, 7183 (1982).
- ²⁵R. D. Bringans and H. Höchst, *Phys. Rev. B* **30**, 5416 (1984).
- ²⁶R. G. Lye and E. M. Logothetis, *Phys. Rev.* **147**, 622 (1966).
- ²⁷J. F. Alward, C. Y. Fong, M. El-Batanouny, and F. Wooten, *Phys. Rev. B* **12**, 1105 (1975).
- ²⁸A. Schlegel, P. Wachter, J. J. Nickl, and H. Lingg, *J. Phys. C* **10**, 4899 (1977).
- ²⁹D. W. Lynch, C. G. Olson, D. J. Peterman, and J. H. Weaver, *Phys. Rev. B* **22**, 3991 (1980).
- ³⁰J. Rivory, J. M. Behaghel, S. Berthier, and J. Lafait, *Thin Solid Films* **78**, 161 (1981).
- ³¹B. Karlsson, J.-E. Sundgren, and B.-O. Johansson, *Thin Solid Films* **87**, 181 (1982).
- ³²L. Roux, J. Hanus, J. C. Francois, and M. Sigrist, *Solar Energy Mater.* **7**, 299 (1982).
- ³³F. A. Modine, R. W. Major, T. W. Haywood, G. R. Gruzalski, and D. Y. Smith, *Phys. Rev. B* **29**, 836 (1984).
- ³⁴F. A. Modine, T. W. Haywood, and C. Y. Allison, *Phys. Rev. B* **32**, 7743 (1985).
- ³⁵C. Y. Allison, F. A. Modine, and R. H. French, *Phys. Rev. B* **35**, 2573 (1987).
- ³⁶L. Ramqvist, *J. Appl. Phys.* **42**, 2113 (1971), and references therein.
- ³⁷V. V. Nemoskalenko, V. P. Krivitskii, A. P. Nesenjuk, L. I. Nikolajev, and A. P. Shpak, *J. Phys. Chem. Solids* **36**, 277 (1975).
- ³⁸V. A. Gubanov, E. Z. Kurmaev, and D. E. Ellis, *J. Phys. C* **14**, 5567 (1981); A. L. Ivanovsky, V. A. Gubanov, G. P. Shveikin, and E. Z. Kurmaev, *J. Less-Common Met.* **78**, 1 (1981).
- ³⁹E. Beauprez, C. F. Hague, J.-M. Mariot, F. Teyssandier, J. Redinger, P. Marksteiner, and P. Weinberger, *Phys. Rev. B* **34**, 886 (1986).
- ⁴⁰J.-M. Mariot, C. F. Hague, W. Lengauer, J. Redinger, P. Weinberger, and E. Beauprez, *Phys. Scr.* **41**, 584 (1990).
- ⁴¹J.-E. Rubensson, N. Wassdahl, G. Bray, J. Rindstedt, R. Nyholm, S. Cramm, N. Mårtensson, and J. Nordgren, *Phys. Rev. Lett.* **60**, 1759 (1988); J. Nordgren, *J. Phys. (Paris) Colloq.* **48**, C9-693 (1987).
- ⁴²J. Pflüger, J. Fink, G. Crecelius, K.-P. Bohnen, and H. Winter, *Solid State Commun.* **44**, 489 (1982).
- ⁴³J. Pflüger, J. Fink, and K. Schwarz, *Solid State Commun.* **55**, 675 (1985).
- ⁴⁴J. Pflüger, J. Fink, W. Weber, K.-P. Bohnen, and G. Crecelius, *Phys. Rev. B* **30**, 1155 (1984); **31**, 1244 (1985).
- ⁴⁵F. Riehle, Th. Wolf, and C. Politis, *Z. Phys. B* **47**, 201 (1982).
- ⁴⁶J. H. Weaver, A. M. Bradshaw, J. F. van der Veen, F. J. Himpsel, D. E. Eastman, and C. Politis, *Phys. Rev. B* **22**, 4921 (1980).
- ⁴⁷L. I. Johansson, A. Callenäs, P. M. Stefan, A. N. Christensen, and K. Schwarz, *Phys. Rev. B* **24**, 1883 (1981); L. I. Johansson, P. M. Stefan, M. L. Shek, and A. N. Christensen, *Solid State Commun.* **36**, 965 (1980).
- ⁴⁸A. Callenäs, L. I. Johansson, A. N. Christensen, K. Schwarz, and J. Redinger, *Phys. Rev. B* **27**, 5934 (1983).
- ⁴⁹A. Callenäs, L. I. Johansson, A. N. Christensen, K. Schwarz, P. Blaha, and J. Redinger, *Phys. Rev. B* **30**, 635 (1984); A. Callenäs, L. I. Johansson, A. N. Christensen, K. Schwarz, and P. Blaha, *ibid.* **32**, 575 (1985).
- ⁵⁰J. Lindström, L. I. Johansson, A. Callenäs, D. S. L. Law, and A. N. Christensen, *Phys. Rev. B* **35**, 7891 (1987).
- ⁵¹P. A. P. Lindberg, L. I. Johansson, J. B. Lindström, and D. S. L. Law, *Phys. Rev. B* **36**, 939 (1987).
- ⁵²P. A. P. Lindberg, P. L. Wincott, L. I. Johansson, and A. N. Christensen, *Phys. Rev. B* **36**, 4681 (1987); P. A. P. Lindberg, P. L. Wincott, and L. I. Johansson, *Surf. Sci.* **189/190**, 761 (1987).

- ⁵³P. A. P. Lindberg, L. I. Johansson, and A. N. Christensen, *Surf. Sci.* **192**, 353 (1987); P. A. P. Lindberg and L. I. Johansson, *ibid.* **192**, 366 (1987).
- ⁵⁴P. A. P. Lindberg and L. I. Johansson, *Z. Phys. B* **68**, 83 (1987).
- ⁵⁵P. A. P. Lindberg, L. I. Johansson, J. B. Lindström, P. E. S. Persson, D. S. L. Law, and A. N. Christensen, *Phys. Rev. B* **36**, 6343 (1987).
- ⁵⁶P. A. P. Lindberg, L. I. Johansson, J. B. Lindström, and D. S. L. Law, *Surf. Sci.* **189/190**, 751 (1987); P. A. P. Lindberg and L. I. Johansson, *Z. Phys. B* **68**, 73 (1987).
- ⁵⁷J. Lindström, P. A. P. Lindberg, L. I. Johansson, D. S. L. Law, and A. N. Christensen, *Phys. Rev. B* **36**, 9514 (1987).
- ⁵⁸J. Lindström, L. I. Johansson, P. E. S. Persson, A. Callenäs, D. S. L. Law, and A. N. Christensen, *Phys. Rev. B* **39**, 3599 (1989); J. Lindström, L. I. Johansson, P. E. S. Persson, and A. Callenäs, *Z. Phys. B* **74**, 451 (1989).
- ⁵⁹K. Edamoto, S. Maehama, E. Miyazaki, and H. Kato, *Phys. Rev. B* **39**, 7461 (1989).
- ⁶⁰J. Garbe and J. Kirschner, *Phys. Rev. B* **39**, 6115 (1989).
- ⁶¹P. L. Wincott, K. L. Håkansson, and L. I. Johansson, *Surf. Sci.* **211/212**, 404 (1989).
- ⁶²K. Schwarz and N. Rösch, *J. Phys. C* **9**, L433 (1976).
- ⁶³G. Ries and H. Winter, *J. Phys. F* **10**, 1 (1980).
- ⁶⁴Yu. N. Kucherenko, L. M. Sheludchenko, V. Z. Khrinovskiy, and V. V. Nemoshkalenko, *J. Phys. Chem. Solids* **45**, 319 (1984).
- ⁶⁵J. E. Lowther and A. Andriotis, *J. Phys. Chem. Solids* **48**, 713 (1987).
- ⁶⁶J. Redinger, R. Eibler, P. Herzig, A. Neckel, R. Podloucky, and E. Wimmer, *J. Phys. Chem. Solids* **46**, 383 (1985); **47**, 387 (1986).
- ⁶⁷P. Herzig, J. Redinger, R. Eibler, and A. Neckel, *J. Solid State Chem.* **70**, 281 (1987).
- ⁶⁸V. P. Zhukov and V. A. Gubanov, *J. Phys. Chem. Solids* **48**, 187 (1987).
- ⁶⁹V. P. Zhukov, V. A. Gubanov, O. Jepsen, N. E. Christensen, and O. K. Andersen, *J. Phys. Chem. Solids* **49**, 841 (1988).
- ⁷⁰J. Klima, *J. Phys. C* **12**, 3691 (1979).
- ⁷¹B. M. Klein, D. A. Papaconstantopoulos, and L. L. Boyer, *Phys. Rev. B* **22**, 1946 (1980).
- ⁷²J. Klima, G. Schadler, P. Weinberger, and A. Neckel, *J. Phys. F* **15**, 1307 (1985); G. Schadler, P. Weinberger, A. Gonis, and J. Klima, *ibid.* **15**, 1675 (1985).
- ⁷³P. Marksteiner, P. Weinberger, A. Neckel, R. Zeller, and P. H. Dederichs, *Phys. Rev. B* **33**, 812 (1986); **33**, 6709 (1986).
- ⁷⁴J. Redinger, P. Marksteiner, and P. Weinberger, *Z. Phys. B* **63**, 321 (1986).
- ⁷⁵G. H. Schadler, A. M. Boring, P. Weinberger, and A. Gonis, *Phys. Rev. B* **38**, 9538 (1988).
- ⁷⁶P. Pecheur, G. Toussaint, and E. Kauffer, *Phys. Rev. B* **29**, 6606 (1984).
- ⁷⁷W. E. Pickett, B. M. Klein, and R. Zeller, *Phys. Rev. B* **34**, 2517 (1986).
- ⁷⁸A. L. Ivanovsky, V. I. Anisimov, D. L. Novikov, A. I. Lichtenstein, and V. A. Gubanov, *J. Phys. Chem. Solids* **49**, 465 (1988).
- ⁷⁹M. Aono, Y. Hou, R. Souda, C. Oshima, S. Otani, and Y. Ishizawa, *Phys. Rev. Lett.* **50**, 1293 (1983); C. Oshima, M. Aono, T. Tanaka, S. Kawai, S. Zaima, and Y. Shibata, *Surf. Sci.* **102**, 312 (1981).
- ⁸⁰S. Otani, T. Tanaka, and Y. Ishizawa, *J. Cryst. Growth* **62**, 211 (1983); Y. Hou, S. Otani, T. Tanaka, and Y. Ishizawa, *ibid.* **68**, 733 (1984).
- ⁸¹T. Miyahara, S. Suzuki, T. Hanyu, H. Kato, K. Naito, H. Fukutani, I. Nagakura, H. Sugawara, S. Nakai, T. Ishii, H. Noda, T. Namioka, and T. Sasaki, *Jpn. J. Appl. Phys.* **24**, 293 (1985).
- ⁸²H. E. Bennett and J. O. Porteus, *J. Opt. Soc. Am.* **51**, 123 (1961).
- ⁸³M. Yanagihara, M. Niwano, T. Koide, S. Sato, T. Miyahara, Y. Iguchi, S. Yamaguchi, and T. Sasaki, *Appl. Opt.* **25**, 4586 (1986).
- ⁸⁴S. Kim and R. S. Williams, *J. Phys. Chem. Solids* **49**, 1307 (1988).